Lithium Battery Materials Li*M*PO$_4$ (*M* = Mn, Fe, Co, and Ni): Insights into Defect Association, Transport Mechanisms, and Doping Behavior

Craig A. J. Fisher, Veluz M. Hart Prieto, and M. Saiful Islam*

Department of Chemistry, University of Bath, Bath, BA2 7AY, United Kingdom

Received May 10, 2008. Revised Manuscript Received July 9, 2008

The defect chemistry, doping behavior, and ion migration in olivine-type materials Li*M*PO$_4$ (*M* = Mn, Fe, Co, and N) are investigated by atomistic simulation techniques. The most favorable intrinsic defect type is found to be the cation antisite defect, in which Li and *M* ions exchange positions. Li migration is found to occur preferentially down [010] channels, following a curved trajectory. Defect association or binding energies for pair clusters composed of combinations of lithium vacancies, antisite cations, and small polaron species are investigated. Migration energies for divalent antisite cations on Li sites suggest that such defects would impede Li diffusion in Li*M*PO$_4$ to varying degrees. Calculation of dopant substitution energies for cations with charges +1 to +5 indicate that supervalent doping (e.g., Ga^{3+}, Ti^{4+}, Nb^{5+}) on either Li or *M* sites is energetically unfavorable and does not result in a large increase in electronic (small polaron) species.

1. Introduction

There is intensive research activity into alternative electrode materials for the next generation of rechargeable lithium-ion batteries, particularly for use in hybrid electric vehicles.[1,2] Olivine-structured orthophosphates Li*M*PO$_4$ (*M* = Mn, Fe, Co, and Ni) have been proposed as viable alternatives to the conventional cathode material, $LiCoO_2$.[1−3] These olivine phosphates have good thermal stability, with high voltages versus the Li^+/Li couple.[4] Moreover, the Fe and Mn members are environmentally benign and of low cost.

To date, most interest has focused on the $LiFePO_4$ phase,[1−3] which is already in commercial use. Attention continues to be paid to the other transition metal systems,[4−8] because any one of these would provide higher cell voltages than $LiFePO_4$. Unfortunately these materials all suffer from a number of drawbacks that must be overcome before they can compete with $LiFePO_4$. For example, $LiMnPO_4$ has poorer Li-ion conductivity than $LiFePO_4$,[5] while the high upper charge voltages of $LiCoPO_4$ and $LiNiPO_4$ mean that significant advances in electrolyte chemistry must be made before they can be put to use.[6,7] $LiNiPO_4$ also exhibits extremely poor electronic conductivity and extremely low charge/discharge capacity.[6]

Low intrinsic electronic conductivity is one of the main difficulties of using all the Li*M*PO$_4$ (*M* = Mn, Fe, Co, and Ni) materials. Typically this is overcome through a combination of synthesis methods, such as preparing the material in nanoparticulate form with a coating of an electronically conductive phase such as carbon.[2,9,10] In the case of $LiFePO_4$, initial reports of supervalent cation doping[11] promised marked improvements in electronic conductivity of 8 orders of magnitude. However, subsequent studies suggest that this is not a true lattice doping effect but a result of carbon contamination from organic precursors and/or metallic-type conductive (secondary) phases being formed on particle surfaces under the highly reducing conditions used.[12−14] Similar conclusions have been reached for $LiCoPO_4$,[14,15] $LiMnPO_4$,[14] and $LiNiPO_4$.[13,14]

Many researchers have also examined the electrochemical behavior of solid solutions of these systems, particularly $LiMn_xFe_{1-x}PO_4$.[16−19] Given their similar ionic radii,[20] it

* Corresponding author: e-mail: m.s.islam@bath.ac.uk.

(1) Tarascon, J.-M.; Armand, M. *Nature* **2008**, *451*, 652.
(2) (a) Whittingham, M. S. *Chem. Rev.* **2004**, *104*, 4271. (b) Whittingham, M. S.; Song, Y. N.; Lutta, S.; Zavalij, P. Y.; Chernova, N. A. *J. Mater. Chem.* **2005**, *15*, 3362.
(3) (a) Padhi, A. K.; Nanjundaswamy, K. S.; Goodenough, J. B. *J. Electrochem. Soc.* **1997**, *144*, 1188. (b) Padhi, A. K.; Nanjundaswamy, K. S.; Masquelier, C.; Goodenough, J. B. *J. Electrochem. Soc.* **1997**, *144*, 2581.
(4) Howard, W. F.; Spotnitz, R. M. *J. Power Sources* **2007**, *165*, 887.
(5) Delacourt, C.; Laffont, L.; Bouchet, R.; Wurm, C.; Leriche, J.-B.; Morcrette, M.; Tarascon, J.-M.; Masquelier, C. *J. Electrochem. Soc.* **2005**, *152*, A913.
(6) Wolfenstine, J.; Allen, J. *J. Power Sources* **2004**, *136*, 150.
(7) (a) Amine, K.; Yasuda, H.; Yamachi, M. *Electrochem. Solid-State Lett.* **2000**, *3*, 178. (b) Bramnik, N. N.; Nikolowski, K.; Baehtz, C.; Bramnik, K. G.; Ehrenberg, H. *Chem. Mater.* **2007**, *19*, 908.
(8) Ramana, C. V.; Ait-Salah, A.; Utsunomiya, S.; Becker, U.; Mauger, A.; Gendron, F.; Julien, C. M. *Chem. Mater.* **2006**, *18*, 3788.
(9) Jin, B.; Gu, H.-B.; Kim, K.-W. *J. Solid State Electrochem.* **2008**, *12*, 105.
(10) (a) Delacourt, C.; Wurm, C.; Reale, P.; Morcrette, M.; Masquelier, C. *Solid State Ionics* **2004**, *173*, 113. (b) Gabrisch, H.; Wilcox, J. D.; Doeff, M. M. *Electrochem. Solid-State Lett.* **2006**, *9*, A360.
(11) Chung, S.-Y.; Bloking, J. T.; Chiang, Y.-M. *Nat. Mater.* **2002**, *1*, 123.
(12) Delacourt, C.; Wurm, C.; Laffont, L.; Leriche, J. B.; Masquelier, C. *Solid State Ionics* **2006**, *177*, 333.
(13) (a) Ravet, N.; Abouimrane, A.; Armand, M. *Nat. Mater.* **2003**, *2*, 702. (b) Subramanya Herle, P.; Ellis, B.; Coombs, N.; Nazar, L. F. *Nat. Mater.* **2004**, *3*, 147.
(14) Ellis, B.; Subramanya Herle, P.; Rho, Y.-H.; Nazar, L. F.; Dunlap, R.; Perry, L. K.; Ryan, D. H. *Faraday Discuss.* **2007**, *134*, 119.
(15) Wolfenstine, J. *J. Power Sources* **2006**, *158*, 1431.
(16) Molenda, J.; Ojczyk, W.; Świerczek, K.; Zając, W.; Krok, F.; Dygas, J.; Liu, R.-S. *Solid State Ionics* **2006**, *177*, 2617.

10.1021/cm801262x CCC: $40.75
Published on Web 08/26/2008

might be expected that these four transition metals are mutually soluble within each system. In the case of $LiCo_xFe_{1-x}PO_4$, neutron diffraction revealed that the Co^{2+} ions are distributed randomly over Fe^{2+} sites.[21] Similarly, in our previous paper, we presented support for the solubility of Mn^{2+}, Co^{2+}, and Ni^{2+} on the Fe site in the $LiFePO_4$ system based on lattice energetics of dopant incorporation.[22]

To understand the processes and structural features influencing the electrochemical behavior of these olivine phosphates, it is clear that fundamental knowledge of the underlying defect and transport properties is needed on the atomic scale. For instance, there has been recent speculation about the possibility of antisite defects and/or defect association (trapping) in $LiFePO_4$ affecting the diffusion behavior.[23,24] Although such atomic level analysis is difficult to perform experimentally, atomistic simulation techniques provide a powerful means of investigating these key solid-state issues.

The present work extends our previous simulation studies of $LiFePO_4$, where we examined the bulk defect chemistry and lithium transport[22] and, more recently, surface structures and crystal morphology.[25] Here we present a systematic comparison of the energetics of intrinsic disorder, defect association, dopant incorporation, Li migration, and antisite cation migration in the four olivine-type materials $LiMPO_4$ (M = Mn, Fe, Co, and Ni).

2. Simulation Methods

This investigation uses well-established simulation techniques based on the Born model of solids. As these techniques are described in detail elsewhere,[26] only a general outline will be given here. All systems were treated as crystalline solids, with interactions between ions consisting of a long-range Coulombic component and a short-range component representing electron−electron repulsion and van der Waals interactions. The short-range interactions were modeled by use of the Buckingham potential:

$$\Phi_{ij}(r_{ij}) = A_{ij}\exp(-r_{ij}/\rho_{ij}) - C_{ij}/r_{ij}^{6} \quad (1)$$

where r is the interatomic separation and A, ρ, and C are ion−ion potential parameters. An additional three-body term was used for the PO_4 units to take into account the angle-dependent nature and rigidity of O−P−O bonds, as used previously for $LiFePO_4$[22,25] and other phosphates.[27] The three-body term took the form of a harmonic angle-bending potential about the P ion:

$$\Phi_{ijk} = \frac{1}{2}K_{ijk}(\theta - \theta_0)^2 \quad (2)$$

where K is the force constant and the angle θ_0 is the equilibrium bond angle for a PO_4 tetrahedron.

To provide a simple means of including effects of electronic polarization, we employed the shell model[25] for M^{2+} and O^{2-} ions. This method allows the polarization effects of charged defects to be taken into account and has proven effective in simulating dielectric properties of a wide range of ceramic oxides. As argued previously,[26] employing a formal charge model does not necessarily mean that the electron distribution corresponds to a fully ionic system, as the validity of the potential model is assessed primarily by its ability to reproduce observed crystal properties. In practice it is found that such models work well, even for compounds where there is undoubtedly a degree of covalency, such as aluminophosphates[27] and olivine silicates.[28] A key benefit of the formal charge model is that there are no ambiguities about the charge state when isovalent and aliovalent dopant substitution are considered.

The lattice relaxation about point defects, defect clusters, or migrating ions was calculated by an implementation of the Mott−Littleton scheme incorporated in the GULP code.[29] This method partitions a crystal lattice into two regions, with ions within the inner spherical region (on the order of >700 ions) immediately surrounding the defect relaxed explicitly. Relaxation of such a large number of ions is important for charge defects that introduce long-range electrostatic pertubations and is not easily treated by electronic structure methods. The outer region extends to infinity, with the outer lattice relaxation treated by quasi-continuum methods, since the defect forces here are relatively weak.

These techniques have been used successfully on a wide range of inorganic solids, including recent work on the fuel cell material $LaBaGaO_4$,[30] as well as spinel-type lithium battery materials $LiMn_2O_4$ and Fe_3O_4.[31]

3. Results and Discussion

3.1. Structural Modeling. The starting point of the study was to reproduce the experimentally observed crystal structures.[32−34] The olivine structure exhibited by $LiMPO_4$ materials is orthorhombic (space group *Pnma*), and consists of PO_4 tetrahedra with M^{2+} ions on corner-sharing octahedral positions (4*c* sites in Wyckoff notation) and Li^+ ions on edge-sharing octahedral positions (4*a* sites), the latter running parallel to the *b* axis. Most of the interatomic potentials were taken from our previous work on $LiFePO_4$, while those for

(17) Yamada, A.; Takei, Y.; Koizumi, H.; Sonoyama, N.; Kanno, R.; Itoh, K.; Yonemura, M.; Kamiyama, T. *Chem. Mater.* **2006**, *18*, 804.
(18) Chang, X.-Y.; Wang, Z.-X.; Li, X.-H.; Zhang, L.; Guo, H.-J.; Peng, W.-J. *Mater. Res. Bull.* **2005**, *40*, 1513.
(19) Burba, C. M.; Frech, R. *J. Power Sources* **2007**, *172*, 870.
(20) Shannon, R. D. *Acta Crystallogr. A* **1976**, *32*, 751.
(21) Nytén, A.; Thomas, J. O. *Solid State Ionics* **2006**, *177*, 1327.
(22) Islam, M. S.; Driscoll, D. J.; Fisher, C. A. J.; Slater, P. R. *Chem. Mater.* **2005**, *17*, 5085.
(23) Maier, J.; Amin, R. *J. Electrochem. Soc.* **2008**, *155*, A339.
(24) Chen, J.; Vacchio, M. J.; Wang, S.; Chernova, N.; Zavalij, P. Y.; Whittingham, M. S. *Solid State Ionics* **2008**, *178*, 1676.
(25) Fisher, C. A. J.; Islam, M. S. *J. Mater. Chem.* **2008**, *18*, 1209.
(26) Catlow, C. R. A. *Computer Modelling in Inorganic Crystallography*; Academic Press: San Diego, CA, 1997.
(27) Henson, N. J.; Cheetham, A.; Gale, J. D. *Chem. Mater.* **1996**, *8*, 664.
(28) Walker, A. M.; Wright, K.; Slater, B. *Phys. Chem. Minerals* **2003**, *30*, 536.
(29) Gale, J. D.; Rohl, A. L. *Mol. Simul.* **2003**, *29*, 291.
(30) Kendrick, E.; Kendrick, J.; Knight, K. S.; Islam, M. S.; Slater, P. R. *Nat. Mater.* **2007**, *6*, 871.
(31) (a) Ammundsen, B.; Rozière, J.; Islam, M. S. *J. Phys. Chem. B* **1997**, *103*, 5175. (b) Islam, M. S.; Catlow, C. R. A. *J. Solid State Chem.* **1988**, *77*, 180.
(32) García-Moreno, O.; Alvarez-Vega, M.; García-Alvarado, F.; García-Jaca, J.; Gallardo-Amores, J. M.; Sanjuán, M. L.; Amador, U. *Chem. Mater.* **2001**, *13*, 1570.
(33) Rousse, G.; Rodriguez-Carvajal, J.; Patoux, S.; Masquelier, C. *Chem. Mater.* **2003**, *15*, 4082.
(34) Kubel, F. *Z. Kristallogr.* **1994**, *209*, 755.

Table 1. Short-Range Potential Parameters

(a) Two-Body

interaction	A (eV)	ρ (Å)	C (eV·Å^6)	Y (e)[a]	k (eV·Å^{-2})[b]
Li^+-O^{2-}	632.1018	0.2906	0.0	1.0	9999.0
$Mn^{2+}-O^{2-}$	2601.394	0.278	0.0	3.42	95.0
$Fe^{2+}-O^{2-}$	1105.2409	0.3106	0.0	2.997	19.26
$Co^{2+}-O^{2-}$	1670.2416	0.2859	0.0	3.503	110.5
$Ni^{2+}-O^{2-}$	1760.0	0.28	0.0	2.0	93.7
$P^{5+}-O^{2-}$	897.2648	0.358 98	0.0	5.0	9999.0
$O^{2-}-O^{2-}$	22 764.3	0.149	44.53	−2.96	65.0

(b) Three-Body

bond type	K (eV·rad^{-2})	θ_0 (deg)
$O^{2-}-P^{5+}-O^{2-}$	1.322 626	109.47

[a] Shell charge. [b] Core−shell spring constant.

Table 2. Calculated and Experimental Structural Parameters of $LiMPO_4$ (M = Mn, Fe, Co, and Ni)

	a (Å)	b (Å)	c (Å)
	$LiMnPO_4$		
calc	10.5401	6.0874	4.6878
expt[a]	10.4310	6.0947	4.7366
Δ	0.1109	−0.0073	−0.0488
	$LiFePO_4$		
calc	10.3713	6.0216	4.6695
expt[b]	10.3377	6.0112	4.6950
Δ	0.0336	−0.0104	−0.0255
	$LiCoPO_4$		
calc	10.2428	5.9093	4.6418
expt[c]	10.2001	5.9199	4.6900
Δ	0.0428	−0.0106	−0.0482
	$LiNiPO_4$		
calc	10.1353	5.8432	4.6257
expt[a]	10.0275	5.8537	4.6763
Δ	0.1078	−0.0105	0.0506

[a] Reference 32. [b] Reference 33. [c] Reference 34.

$Mn^{2+}-O^{2-}$, $Co^{2+}-O^{2-}$, and $Ni^{2+}-O^{2-}$ interactions were obtained by refining parameters from previous studies of their corresponding binary oxides. The potential parameters resulting from these refinements are listed in Table 1, with comparisons between the calculated unit cell parameters and those of the experimental crystal structures given in Table 2.

The calculated unit cell parameters deviate from experiment by at most 0.11 Å (in the case of $LiMnPO_4$) and in most cases much less; the same is found for the Li−O, M−O, and P−O bond lengths (see Supporting Information). As is observed experimentally, the simulated lattice parameters and unit cell volumes decrease across the series Mn, Fe, Co, Ni in accordance with Vegard's law. This, combined with the excellent reproduction of the relatively complex olivine crystal structure, gives us confidence that the interatomic potential model can be used reliably in subsequent defect, dopant, and migration calculations.

3.2. Intrinsic Atomic Defects. A series of isolated point defect (vacancy and interstitial) energies were calculated for both systems. By combining these energies, the relative energies of formation of Frenkel and Schottky-type defects were determined. These take the following general forms (using Kröger−Vink notation), where $M = Mn^{2+}$, Fe^{2+}, Co^{2+}, or Ni^{2+}:

$$\text{Li Frenkel:} \quad Li_{Li}^{\times} \rightarrow V_{Li}' + Li_i^{\bullet} \tag{3}$$

$$M \text{ Frenkel:} \quad M_M^{\times} \rightarrow V_M'' + M_i^{\bullet\bullet} \tag{4}$$

$$\text{O Frenkel:} \quad O_O^{\times} \rightarrow V_O^{\bullet\bullet} + O_i'' \tag{5}$$

$$\text{Schottky:} \quad Li_{Li}^{\times} + M_M^{\times} + P_P^{\times} + 4O_O^{\times} \rightarrow V_{Li}' + V_M'' + V_P'''' + 4V_O^{\bullet\bullet} + LiMPO_4 \tag{6}$$

$$Li_2O \text{ Schottky-like:} \quad 2Li_{Li}^{\times} + O_O^{\times} \rightarrow 2V_{Li}' + V_O^{\bullet\bullet} + Li_2O \tag{7}$$

$$MO \text{ Schottky-like:} \quad M_M^{\times} + O_O^{\times} \rightarrow V_M'' + V_O^{\bullet\bullet} + MO \tag{8}$$

We also examined the Li/M "antisite" pair defect, which involves the exchange of an Li^+ ion (radius 0.74 Å) with an M^{2+} ion (Mn^{2+} radius 0.83 Å, Fe^{2+} radius 0.78 Å, Co^{2+} radius 0.75 Å, and Ni radius 0.69 Å), according to

$$Li_{Li}^{\times} + M_M^{\times} \rightarrow Li_M' + M_{Li}^{\bullet} \tag{9}$$

This type of defect is worth investigating since antisite or cation-exchange effects have been observed in the isostructural olivine silicates.[35]

Off-stoichiometry defects (lithium deficiency or transition metal excess) were also considered according to

$$2Li_{Li}^{\times} + \frac{1}{2}O_2 \rightarrow 2V_{Li}' + 2h^{\bullet} + Li_2O \tag{10}$$

$$MO + 2Li_{Li}^{\times} \rightarrow M_{Li}^{\bullet} + V_{Li}' + Li_2O \tag{11}$$

Our approach to electronic defects follows that used for other oxides (e.g., $LiMn_2O_4$ spinel[31]) in which we model the localized hole ($h^{\bullet}$) species (small polaron) on the transition metal ion as M^{3+} (see Supporting Information for details). Combining the calculated energies of isolated point defects and lattice energies, we can derive the energies for these intrinsic defect processes (eqs 3−11).

Examination of the results in Table 3 reveals three main points. First, the magnitude of the calculated energies suggests formation of M Frenkel, O Frenkel and Schottky defects is unfavorable. In particular, oxygen vacancies, oxygen interstitials, M^{2+} vacancies, and M^{2+} interstitials are highly unfavorable and thus unlikely to occur in any significant concentration.

Second, the most favorable intrinsic defect for all $LiMPO_4$ materials is the Li/M antisite pair (energy <1.50 eV), as predicted in our earlier study of $LiFePO_4$.[22] This suggests that even at low temperatures there will be a small percentage of Li ions on M sites and M ions on Li sites; the concentration would be temperature-dependent and hence sensitive to experimental synthesis conditions. Structural analysis of hydrothermally synthesized $LiFePO_4$ suggests 3 mol % Fe on the lithium sites,[24] while a recently reported scanning transmission electron microscopy (STEM) study[36] confirms

(35) (a) Henderson, C. M. B.; Knight, K. S.; Redfern, S. A. T.; Wood, B. J. *Science* **1996**, *271*, 1713. (b) Henderson, C. M. B.; Redfern, S. A. T.; Smith, R. I.; Knight, K. S.; Charnock, J. M. *Am. Mineral.* **2001**, *86*, 1170.

(36) Chung, S.-Y.; Choi, S.-Y.; Yamamoto, T.; Ikuhara, Y. *Phys. Rev. Lett.* **2008**, *100*, 125502.

Table 3. Energies of Intrinsic Atomic Defects in Li*M*PO$_4$ (*M* = Mn, Fe, Co, and Ni)

		energy (eV)			
disorder type	eq	Mn	Fe	Co	Ni
Li Frenkel	3	1.97	2.15	2.32	2.38
M Frenkel	4	6.80	5.58	6.29	6.35
O Frenkel	5	7.32	5.46	6.71	8.65
full Schottky	6	33.58	25.30	29.96	33.20
Li_2O Schottky-like	7	7.36	6.33	6.97	6.95
*M*O Schottky-like	8	7.15	5.58	6.21	6.77
Li/*M* antisite	9	1.48	1.13	1.18	1.17
Li^+ deficiency	10	8.97	4.41	5.27	7.58
M^{2+}excess	11	3.14	3.13	3.38	3.55

our earlier prediction of antisite defects in $LiFePO_4$, quoting a concentration of around 1%. Our present results demonstrate that such defects are general to the olivine-type phosphates Li*M*PO$_4$.

Such cation exchange is well-known in olivine silicates such as $MgFeSiO_4$[35] and can be rationalized in terms of the similar volumes and coordination environments of the two cation sites. In the Li*M*PO$_4$ materials, however, one consequence of this exchange is that an *M* ion on an Li site could block the lithium diffusion pathway, a point we return to in section 3.5.

Interestingly, in the Na analogue of the iron-containing system, $NaFePO_4$, the positions of the Na^+ and Fe^{2+} ions are completely reversed (i.e., all Fe^{2+} are on 4*a* sites with the larger Na^+ ion on 4*c* sites).[37] Consequently $NaFePO_4$ has very poor ionic conductivity, as the 4*c* sites on which the Na^+ ions reside do not form a continuous network, unlike the 4*a* sites aligned along the [010] direction. This is also consistent with the low energies calculated for Na^+ substitution in Li*M*PO$_4$ materials (see section 3.6).

Finally, the second lowest energies for all Li*M*PO$_4$ systems are found for the Li Frenkel defect (Table 3). This suggests that a minor population of such defects could be present at high temperatures. We note that intrinsic redox processes such as oxidation, reduction, and disproportionation were also considered. In general, the energies (all greater than 3.2 eV) suggest that oxidation (with $V_{Li}^{'}$ and M^{3+} formation) and reduction (with $V_O^{\bullet\bullet}$ and M^+ formation) of the olivine phosphate materials is difficult. This is consistent with the observation that these materials exhibit low intrinsic electronic conduction and that they do not show the oxygen nonstoichiometry found in other oxide cathode materials such as $Li_2MnO_{3-\delta}$.[38]

3.3. Defect Association. It is well established that the electrostatic and elastic interactions between point defects can lead to clustering or association. In the field of oxide-ion conductors in particular, it is known that defect clustering can add a binding (association) energy term to the conduction activation energy. For example, experimental and calculated binding energies for defect pair clusters in lanthanide-doped CeO_2 for use in solid oxide fuel cells fall in the range −0.1 to −0.6 eV.[39]

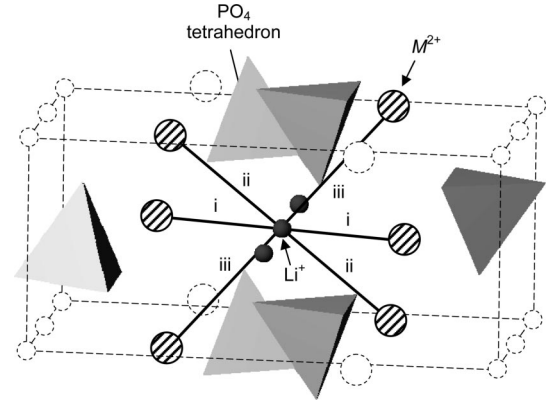

Figure 1. Cation neighbors relative to an Li site, showing three pairs of nonequivalent Li−*M* distances (Roman numerals indicate increasing interatomic distance), and surrounded by PO_4 tetrahedra. The other cations and unit cell are shown with dashed lines for clarity.

As there are a number of possible defects in the olivine orthophosphate systems, depending on temperature, initial stoichiometries, and lithium activity, several pair configurations of oppositely charged defects were considered. Indeed, the defect chemistry and possible association (trapping) in $LiFePO_4$ have been discussed recently by Maier and Amin,[23] where they note that detailed atomistic modeling is required to quantify the energies involved.

As demonstrated by previous studies on complex oxides,[26,40] our simulation methods can model accurately the electrostatic, polarization, and elastic strain energies, which are the predominant terms in any local association process. The clusters considered comprised combinations of antisite defects, lithium vacancies, and hole species in the Li*M*PO$_4$ (M = Mn, Fe, Co, and Ni) systems.

The cluster binding energies (E_{bind}) were calculated from the general relationship

$$E_{bind} = E_{cluster} - \sum_{component} E_{isolated} \qquad (12)$$

where a negative value indicates that the cluster is stable with respect to the isolated component defects. Energies of pairs of the most energetically favorable defects on neighboring cation sites were calculated relative to the same number of isolated defects. The defect pair clusters considered were

(a) Li/*M* antisite defects, $[Li_M^{'} - M_{Li}^{\bullet}]$
(b) *M* ion on an Li site and a lithium vacancy, $[M_{Li}^{\bullet} - V_{Li}^{'}]$
(c) M^{3+} hole center (small polaron) and a lithium vacancy, $[M_M^{\bullet} - V_{Li}^{'}]$

There are three nonequivalent Li−*M* interatomic distances to consider for configurations a and b (Figure 1). The lowest energies for each cluster type, listed in Table 4, were found for the shortest separation between defects.

Three key points can be identified from the results. First, all antisite clusters had negative binding energies, indicating that they are more stable than the isolated defects. This suggests that antisite defects will aggregate in the material, acting as precursors to larger clusters, as has recently been

(37) Bridson, J. N.; Quinlan, S. E.; Tremaine, P. R. *Chem. Mater.* **1998**, *10*, 763.
(38) Pasero, D.; McLaren, V.; de Souza, S.; West, A. R. *Chem. Mater.* **2005**, *17*, 345.
(39) (a) Catlow, C. R. A. *J. Chem. Soc., Faraday Trans.* **1990**, *86*, 1167. (b) Kilner, J. A. *Solid State Ionics* **2000**, *129*, 13.
(40) Mather, G. C.; Islam, M. S.; Figueirido, F. M. A. *Adv. Funct. Mater.* **2007**, *17*, 905.

Table 4. Binding Energies of Defect Pair Clusters on Neighboring Cation Sites in LiMPO$_4$ (M = Mn, Fe, Co, and Ni)

	binding energy (eV)			
defect cluster	Mn	Fe	Co	Ni
$[Li'_M - M^{\bullet}_{Li}]$	−0.57	−0.44	−0.52	−0.54
$[M^{\bullet}_{Li} - V'_{Li}]$	−0.65	−0.48	−0.57	−0.59
$[M^{\bullet}_{M} - V'_{Li}]$	−0.50	−0.39	−0.45	−0.64

observed in $LiFePO_4$.[36] Although the binding energies are very similar for all four transition metals, the $[Li'_{Fe} - Fe^{\bullet}_{Li}]$ pair in $LiFePO_4$ and the $[Li'_{Mn} - Mn^{\bullet}_{Li}]$ pair in $LiMnPO_4$ were the most weakly and strongly bound, respectively.

Second, similar trends are found for clusters involving lithium vacancies and M^{2+} cations on lithium sites. The results reveal significant $[M^{\bullet}_{Li} - V'_{Li}]$ binding, which could lead to trapping of the migrating Li^+ vacancies; as noted, such ions on the lithium site ($M^{\bullet}_{Li}$) could also hinder lithium diffusion along the b-axis channel.[22,24] Because "trapping" introduces a further energy term to the lithium migration energy, this has implications for the lithium conductivity of these materials. The smallest binding energies are again found for the Fe system, which may favor higher lithium conduction rates compared to the others. The greatest trapping is predicted to occur in the $LiMnPO_4$ system. Although it is difficult to draw clear conclusions on the factors that lead to the small differences in binding energies for the four systems, as already mentioned, some of the key factors for defect association are electrostatic, polarization, and elastic strain (ion size) effects.

Finally, we find significant binding energies between the small polaron species (e.g., Fe^{3+} or Mn^{3+}) and lithium vacancies, which are of relevance to the observed electronic conductivity; these results suggests the coupling or trapping of these charge carriers in $Li_{1-x}MPO_4$, as Mössbauer experiments have indicated that electron transport in Li_xFePO_4 occurs by small polaron hopping.[41] Our results are compatible with GGA+U-type calculations that find a hole-vacancy binding energy in $Li_{1-x}FePO_4$ of greater than 500 meV.[42]

3.4. Li Ion Migration. By use of atomistic simulation techniques, it is possible to examine various possible diffusion paths responsible for lithium conduction in these materials. Relaxation of the surrounding lattice (>700 ions) as an ion migrates through the structure is treated explicitly by these defect modeling methods.

Three possible migration paths were examined; these are labeled A−C in Figure 2 in order of shortest to longest jump distance. Path A involves migration between adjacent Li sites in the [010] direction, parallel to the b axis, with a jump distance of 2.9∼3.0 Å. Path B involves migration in the [001] direction, parallel to the c axis, with a jump distance of 4.6∼4.7 Å, while path C involves migration between the lithium channels in the [101] direction with the longest jump distance of 5.6∼5.8 Å. Energy profiles for these mechanisms can be derived by calculating the energy of the migrating ion along the diffusion path, after relaxation of the surrounding ions. The position of highest potential energy along the migration path corresponds to the activation energy of migration, E_{mig}. The migration energies for all compositions are listed in Table 5.

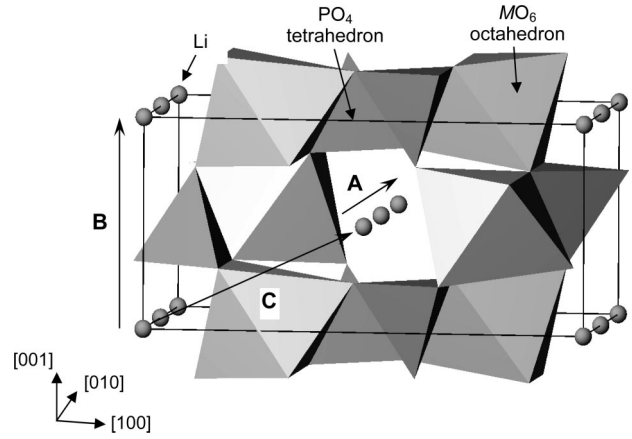

Figure 2. Paths considered for lithium ion migration in olivine-structured phosphates LiMPO$_4$ (M = Mn, Fe, Co, and Ni).

Table 5. Mechanisms and Energies of Li Migration in LiMPO$_4$ (M = Mn, Fe, Co, and Ni)

	migration energy, E_{mig} (eV)			
path[a]	Mn	Fe	Co	Ni
A [010]	0.62	0.55	0.49	0.44
B [001]	2.83	2.89	3.28	3.49
C [101]	2.26	3.36	3.41	3.99

[a] Illustrated in Figure 2.

The results reveal that the lowest energy path for Li ion migration for all four materials is down the [010] channel, path A. High barriers of >2.2 eV are calculated for the other pathways (B and C), indicating that lithium ions cannot readily jump from one channel to another. By way of comparison, similar differences in activation energies are found between oxide ion migration (∼0.9 eV) and cation migration (∼2.3 eV) in the fast oxide ion conductor 8 mol % yttria-stabilized zirconia (YSZ),[43] in which cation migration is known to be orders of magnitude slower than oxide ion migration. This illustrates the strongly anisotropic nature of Li ion migration in the olivine phosphates. Our results are also consistent with electronic structure (density functional theory-type) calculations,[44] although in that study lower energy barriers of 0.1∼0.3 eV were reported. Our calculated energies for $LiFePO_4$ and $LiMnPO_4$ are in accord with experimental activation energies of 0.63 eV for both $LiFePO_4$ and $LiFe_{0.45}Mn_{0.55}PO_4$.[16]

In the context of nanoparticle behavior, our recent $LiFePO_4$ surface simulations[25] showed that the (010) surface is prominent in the crystal morphology, in good agreement with experiment.[45] The exposure of this surface is significant since it is normal to the favored [010] conduction pathway.

Detailed structural analysis of the migrating ion shows that a curved migration path is taken between the adjacent lithium

(41) (a) Ellis, B.; Perry, L. K.; Ryan, D. H.; Nazar, L. F. *J. Am. Chem. Soc.* **2006**, *128*, 11416. (b) Zaghib, K.; Mauger, A.; Goodenough, J. B.; Gendron, F.; Julien, C. M. *Chem. Mater.* **2007**, *19*, 3740.
(42) Maxisch, T.; Zhou, F.; Ceder, G. *Phys. Rev. B* **2006**, *73*, 104301.
(43) Suárez, G.; Garrido, L. B.; Aglietti, E. F. *Mater. Chem. Phys.* **2008**, *110*, 370.
(44) Morgan, D.; Van der Ven, A.; Ceder, G. *Electrochem. Solid-State Lett.* **2004**, *7*, A30.
(45) Dokko, K.; Koizumi, S.; Nakano, H.; Kanamura, K. *J. Mater. Chem.* **2007**, *17*, 4803.

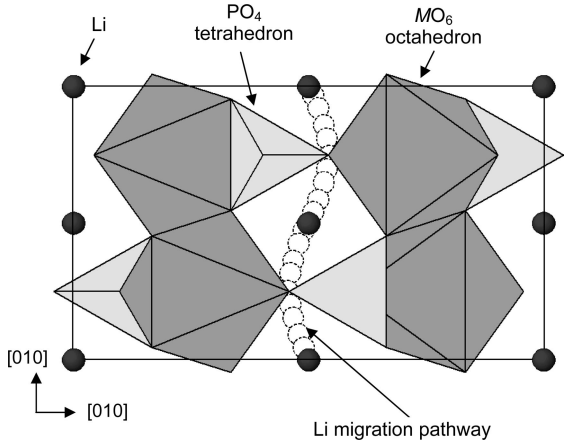

Figure 3. Schematic of curved migration pathway calculated for lithium ion migration in olivine-structured phosphates LiMPO$_4$ (M = Mn, Fe, Co, and Ni).

sites[22] and not a direct linear path, as might be assumed. In each case, the migrating ion deviates from a linear path by around 0.5 Å at its midpoint (Figure 3), while there is also a certain amount of lattice distortion around the diffusing lithium ion as it passes between the PO$_4$ and MO$_6$ polyhedra. More recently, neutron diffraction measurements of LiFePO$_4$ by Yamada et al.[46] confirm one-dimensional Li$^+$ diffusion, with a curved migration pathway between adjacent lithium sites, in excellent agreement with the present simulation results, as well as our earlier prediction.[22] Similarly, magnetic susceptibility and X-ray absorption spectroscopy measurements reveal that the magnetic properties and electronic structure of single-crystal LiFePO$_4$ are different in the three axial directions.[47]

These results contrast with a recent report that lithium ion diffusion in single crystals of LiFePO$_4$ was two-dimensional rather than one-dimensional.[48] However, two-dimensional transport with similar activation energies in the b and c directions is difficult to reconcile with the distinctly anisotropic nature of the orthorhombic olivine structure; for example, the corresponding Li−Li jump distances are highly disparate at 2.9∼3.0 and 4.6∼4.7 Å, respectively. Furthermore, tracer diffusion studies of another olivine-structured material, Fe$_2$SiO$_4$, found Fe diffusion to be different along the three principal axes.[49]

3.5. Antisite Cation Migration. Our defect calculations suggest that Li/M antisite defects are intrinsic to LiMPO$_4$, and there is experimental evidence of a low concentration (<3%) of Fe on Li sites in LiFePO$_4$.[24] It may therefore be difficult to avoid M cations on Li sites blocking the diffusion pathways down [010] channels, unless the antisite defect itself is mobile. Either scenario would likely reduce the electrochemical capacity.

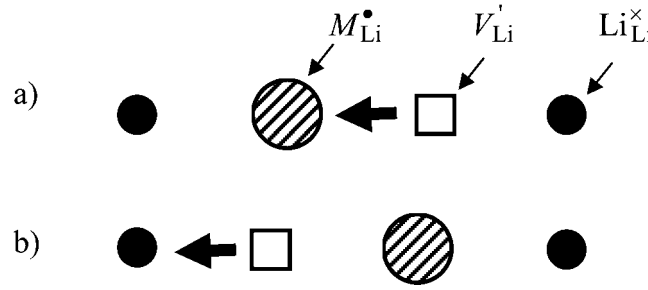

Figure 4. Schematic of two stages in migration of an Li vacancy ($V_{Li}^{'}$) down a [010] channel of LiMPO$_4$ (M = Mn, Fe, Co, and Ni) near an antisite M cation ($M_{Li}^{\bullet}$). (a) Exchange of $V_{Li}^{'}$ and $M_{Li}^{\bullet}$; (b) exchange of $V_{Li}^{'}$ and a lithium ion ($Li_{Li}^{\times}$).

Table 6. Energies of Antisite Cation ($M_{Li}^{\bullet}$) Migration along [010] in LiMPO$_4$ (M = Mn, Fe, Co, and Ni)

mechanism	E_{mig} (eV)
$Mn_{Li}^{\bullet} \rightarrow V_{Li}^{'}$	0.92
$Fe_{Li}^{\bullet} \rightarrow V_{Li}^{'}$	0.70
$Co_{Li}^{\bullet} \rightarrow V_{Li}^{'}$	0.81
$Ni_{Li}^{\bullet} \rightarrow V_{Li}^{'}$	1.33

In order to examine whether antisite defects affect long-range Li diffusion, the energy of migration of the divalent cation between lithium sites was calculated. This process can be viewed as an exchange of an antisite cation ($M_{Li}^{\bullet}$) with a lithium vacancy (as illustrated in Figure 4); the lithium vacancy would then continue to migrate in the opposite direction down the [010] channel. A similar simulation procedure to that for Li migration was used, which allowed the lowest energy migration path to be determined. As for Li$^+$ migration, this was found to be a curved path between 4a sites (Figure 3).

All the calculated migration energies in Table 6 are 0.15∼0.7 eV greater than the corresponding Li migration values, indicating lower antisite cation mobility compared to pure lithium diffusion. This suggests that antisite defects ($M_{Li}^{\bullet}$) would impede Li diffusion to varying degrees down [010] channels. However, the most favorable migration energy (relatively low at 0.7 eV) is for LiFePO$_4$, suggesting that a population of antisite defects in this system would have the least effect on lithium diffusion kinetics.

At this point it is interesting to examine overall trends in the energies of ion migration and defect association for LiMPO$_4$ systems. The magnitudes of the energies listed in Tables 4−6 reveal that the Fe system has a low lithium vacancy migration energy, the weakest [$M_{Li}^{\bullet}-V_{Li}^{'}$] binding energy, and the lowest barrier to antisite cation migration. Combined, these results suggest higher lithium conduction rates in LiFePO$_4$ than in the other three systems.

3.6. Dopant Substitution. Reports that low-level (<3%) doping of LiFePO$_4$ with cations (such as Al^{3+}, Zr^{4+}, and Nb^{5+}) produces orders-of-magnitude improvements in electronic conductivity[11] have stimulated considerable debate about the precise substitution mechanisms, nature of the conductive species, and, crucially, whether the dopant goes into the crystal lattice or if the enhanced conductivity is due to secondary effects such as carbon contamination and/or phosphide formation.[12−14,16]

Our simulation methods can probe these issues by generating quantitative estimates of the relative energies of different

(46) Yamada, A.; Nishimura, S.; Kanno, R.; Kobayashi, Y.; Miyashiro, H.; Yashima, M.; Ohayama, K.; Yamaguchi, Y. *Nat. Mater.* **2008**, in press.
(47) Liang, G.; Park, K.; Li, J.; Benson, R. E.; Vaknin, D.; Markert, J. T.; Croft, M. C. *Phys. Rev. B* **2008**, *77*, 064414.
(48) Amin, R.; Balaya, P.; Maier, J. *Electrochem. Solid-State Lett.* **2007**, *10*, A13.
(49) (a) Aggarwal, S.; Töpfer, J.; Tsai, T.-L.; Dieckmann, R. *Solid State Ionics* **1997**, *321*, 101. (b) Ullrich, K.; Becker, K. D. *Solid State Ionics* **2001**, *307*, 141.

modes of dopant substitution. This can provide a useful systematic guide to the site selectivity for different dopant species and to trends in dopant solubility. In this study we have examined a range of dopants, from monovalent to pentavalent, in LiMPO$_4$, constituting a wider survey than current experimental reports.

For isovalent dopants (such as Na^+ on Li^+ or Mg^{2+} on M^{2+}), no charge-compensating defect is required. However, for aliovalent dopants (whether donor ions such as Mg^{2+} on Li^+ or Al^{3+} on M^{2+}, or acceptor ions such as Na^+ on M^{2+}), the type of charge-compensating mechanism has not been clearly established from experiment and could consist of either Li vacancies, M vacancies, O vacancies, or electronic species (e.g., Fe^+, Fe^{3+}). We therefore calculated the overall substitution energy for a variety of different compensation mechanisms. With Na^+ and Zr^{4+} as example dopant species on both Li and M sites (where $M = Mn^{2+}$, Fe^{2+}, Co^{2+}, or Ni^{2+}), incorporation mechanisms of the following types (normalized to a single dopant ion) were considered:

Li site

$$\text{No compensation:}\quad \tfrac{1}{2}Na_2O + Li_{Li}^{\times} \rightarrow Na_{Li}^{\times} + \tfrac{1}{2}Li_2O \tag{13}$$

$$Li^+ \text{ vacancy:}\quad ZrO_2 + 4Li_{Li}^{\times} \rightarrow Zr_{Li}^{\bullet\bullet\bullet} + 3V_{Li}' + 2Li_2O \tag{14}$$

$$M^{2+} \text{ vacancy:}\quad ZrO_2 + Li_{Li}^{\times} + \tfrac{3}{2}M_M^{\times} \rightarrow Zr_{Li}^{\bullet\bullet\bullet} + \tfrac{3}{2}V_M'' + \tfrac{1}{2}Li_2O + \tfrac{3}{2}MO \tag{15}$$

$$M^+ \text{ (electron) formation:}\quad ZrO_2 + Li_{Li}^{\times} + \rightarrow Zr_{Li}^{\bullet\bullet\bullet} + 3e' + \tfrac{1}{2}Li_2O + \tfrac{3}{4}O_2 \tag{16}$$

M site

$$M^{3+} \text{ (hole) formation:}\quad \tfrac{1}{2}Na_2O + M_M^{\times} + \tfrac{1}{4}O_2 \rightarrow Na_M' + h^{\bullet} + MO \tag{17}$$

$$Li^+ \text{ vacancy:}\quad ZrO_2 + 2Li_{Li}^{\times} + M_M^{\times} \rightarrow Zr_M^{\bullet\bullet} + 2V_{Li}' + Li_2O + MO \tag{18}$$

$$M^{2+} \text{ vacancy:}\quad ZrO_2 + 2M_M^{\times} \rightarrow Zr_M^{\bullet\bullet} + V_M'' + 2MO \tag{19}$$

$$M^+ \text{ (electron) formation:}\quad ZrO_2 + M_M^{\times} \rightarrow Zr_M^{\bullet\bullet} + 2e' + MO + \tfrac{1}{2}O_2 \tag{20}$$

The energies of these dopant substitution or solution reactions were calculated by combining the appropriate defect and lattice energy terms for each equation. Interatomic potentials used to model the corresponding binary oxides of the dopant cations were used in each case (given as Supporting Information). This systematic approach has been applied successfully to other oxide and silicate systems.[40,50]

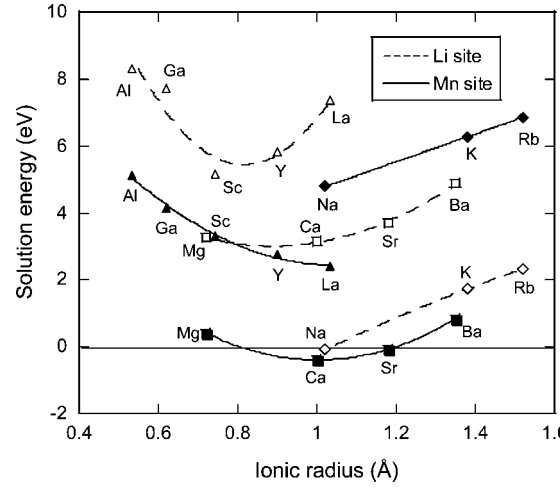

Figure 5. Solution energies versus dopant ionic radius for LiMnPO$_4$. Lines are a guide for the eye only.

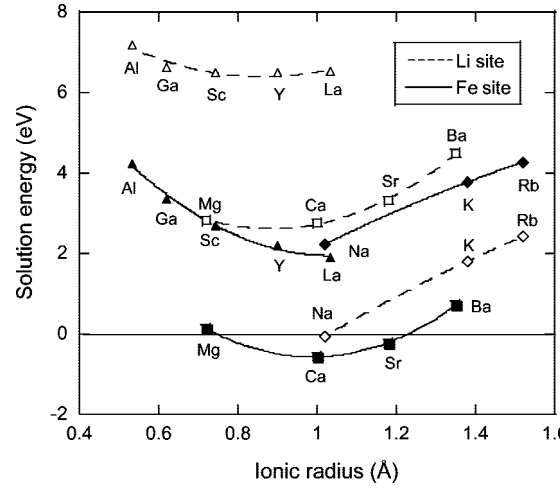

Figure 6. Solution energies versus dopant ionic radius for LiFePO$_4$. Lines are a guide for the eye only

The dopant calculations were also carried out at the dilute limit, as is appropriate for examining low dopant concentrations.

Dopant incorporation, or solution, energies for a range of A^+, A^{2+}, and A^{3+} cation dopants with the most favorable charge compensation mechanisms are plotted as a function of ionic radius in Figures 5−8; because the solution energies for A^{4+} and A^{5+} dopants were much higher, these are listed separately in Table 7. Indeed, Nb^{5+} dopants on M^{2+} sites in LiMnPO$_4$ and LiNiPO$_4$ were found to be completely unstable.

These results indicate two main features. First, in all four LiMPO$_4$ materials the lowest energies are found for isovalent substitution; in particular, only Na doping for Li^+ and divalent doping for M^{2+} were found to be favorable. This is consistent with the observed mutual solubility of Mg^{2+}, Mn^{2+}, Fe^{2+}, Co^{2+}, and Ni^{2+} in the various LiMPO$_4$ systems.[6,15−19,21,24,51] However, these do not require any charge compensation and hence would not increase the number of charge carriers.

For example, Roberts et al.[52] recently showed that Mg^{2+} is fully soluble on Fe sites in LiFePO$_4$ but does not go onto

(50) Tolchard, J. R.; Slater, P. R.; Islam, M. S. *Adv. Funct. Mater.* **2007**, *17*, 2564.

(51) Chen, G.; Richardson, T. J. *J. Electrochem. Soc.* **2008**, in press.

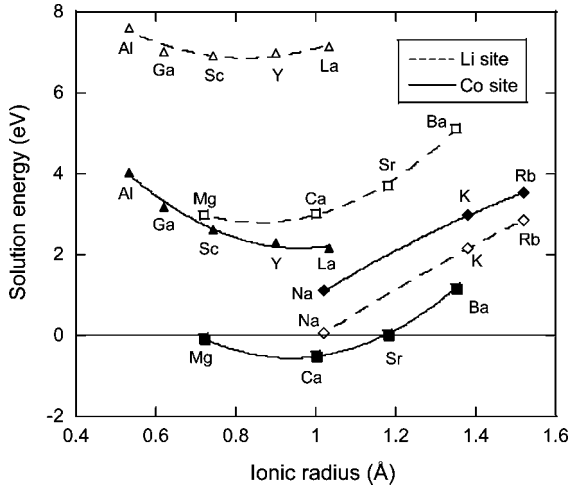

Figure 7. Solution energies versus dopant ionic radius for $LiCoPO_4$. Lines are a guide for the eye only.

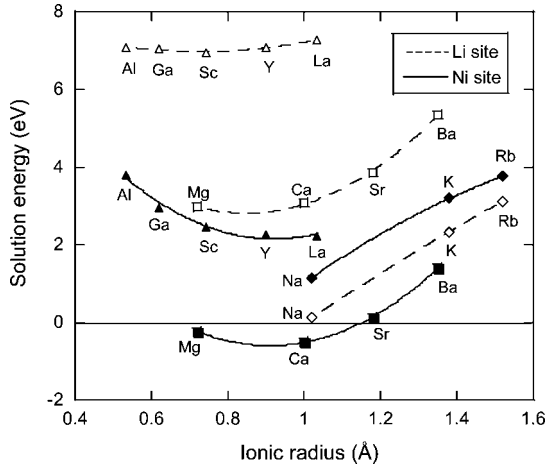

Figure 8. Solution energies versus dopant ionic radius for $LiNiPO_4$. Lines are a guide for the eye only.

Table 7. Solution Energies for Tetra- and Pentavalent Dopants in Li*M*PO_4 (*M* = Mn, Fe, Co, and Ni)

	solution energy (eV/dopant)		
site	Ti^{4+}	Zr^{4+}	Nb^{5+}
	$LiMnPO_4$		
Li	11.0	12.5	17.9
Mn	7.6	6.8	NC[a]
	$LiFePO_4$		
Li	10.7	10.6	13.5
Fe	6.0	5.7	7.7
	$LiCoPO_4$		
Li	11.6	11.5	14.8
Co	6.3	7.3	12.5
	$LiNiPO_4$		
Li	11.8	11.7	15.1
Ni	6.2	5.8	NC[a]

[a] NC = nonconvergence of calculation.

the Li site. The $LiFe_{0.9}Mg_{0.1}PO_4$ system is reported to be more stable to capacity fade than undoped $LiFePO_4$,[24] although the incorporation of redox-inactive Mg^{2+} would reduce the effective electrochemical capacity. Interestingly, our results suggest that the most favorable dopant for M^{2+} is calcium, which to our knowledge has not been widely examined.

Second, a key result is that supervalent doping (especially of A^{4+} and A^{5+} ions) is energetically unfavorable in all Li*M*PO_4 systems. This strongly suggests that these ions are unstable within the crystal lattice and unlikely to be incorporated beyond low concentrations (<3%), in accord with our earlier study on $LiFePO_4$.[22] For each system, the overall trends reveal that the greater the difference between the charges of the dopant and host ion, the higher the dopant incorporation energy (e.g., for the Li site, solution energies increase as $Mg^{2+} < Ga^{3+} < Ti^{4+} < Nb^{5+}$). This indicates that electrostatic interactions dominate the energetics of dopant incorporation in these olivine-structured Li*M*PO_4 materials.

For both Li and *M* sites, the least favorable donor dopants were Ti^{4+} and Nb^{5+}. The compensation mechanism for such supervalent dopants was found to be formation of M^{2+} vacancies, whereas compensation by a change in charge state of the transition metal (i.e., to give an M^{+} small polaron species) was much higher in energy. It is therefore unclear as to how supervalent doping could lead to a dramatic improvement in electronic conductivity.

Maier and Amin[23] also note that even if a small amount of supervalent (donor) dopant could enter the lattice to alter the transition metal's valence state, the number of native electronic carriers (holes) would decrease, effectively lowering the overall electronic conductivity, not increasing it. Furthermore, with suitable processing both $LiFePO_4$ and $LiCoPO_4$ can be made to exhibit conductivities as high as $10^{-4}\sim10^{-2}$ S cm^{-1} in the absence of any dopants, demonstrating that doping need not be a major contributor to any improvements in conductivity.[12,14,16]

Our simulation results also bear out other experimental reports. Butt et al.[53] obtained Raman data showing that Ti^{4+} is insoluble in $LiNiPO_4$, consistent with our results for this dopant. Wolfenstine[15] also demonstrated that the electronic conductivity of $LiCoPO_4$ is not improved by doping, finding that the observed increase is due to the conductive Co_2P layer formed by carbothermal reduction. Delacourt et al.[12] attempted to dope $LiFePO_4$ with Nb^{5+} but were unsuccessful, while Ellis et al.[14] showed that aliovalent dopants Al, Y, Cr, and Zr do not contribute to the high conductivity observed in Li*M*PO_4 treated at high temperatures under carbothermal or reducing conditions.

4. Conclusions

This systematic survey of the cathode materials Li*M*PO_4 (*M* = Mn, Fe, Co, and Ni) used atomistic simulation techniques to provide detailed insights into defect, dopant, and ion migration properties relevant to their electrochemical behavior. The main results can be summarized as follows:

(1) The observed crystal structures of all four phases were successfully reproduced by our potential models. The most favorable intrinsic defect in Li*M*PO_4 systems is the antisite defect, for which a small population (<2%) of Li^{+} and M^{2+}

(52) Roberts, M. R.; Vitins, G.; Owen, J. R. *J. Power Sources* **2008**, *179*, 754.
(53) Butt, G.; Sammes, N.; Tompsett, G.; Smirnova, A.; Yamamoto, O. *J. Power Sources* **2004**, *134*, 72.

ions is expected to exchange sites; this would be temperature-dependent and hence sensitive to experimental synthesis conditions.

(2) Lithium ion diffusion follows a nonlinear, curved trajectory down the [010] channel, with relatively low migration energies (ca. 0.4∼0.6 eV). High barriers of >2.2 eV for other pathways indicate that lithium ions cannot readily span the large jump (>4.5 Å) between channels. This one-dimensional transport mechanism is consistent with the strongly anisotropic nature of the orthorhombic olivine structure.

(3) Defect association effects could have a strong effect on the transport properties of $LiMPO_4$. Association or binding energies of ca. −0.5 eV are found for $[M_{Li}^{\bullet}-V_{Li}^{\prime}]$ pair clusters, which has implications for lithium conductivity as M^{2+} cations on Li sites could lead to trapping of the migrating Li^+ vacancies. Significant binding energies (ca. −0.4 to −0.6 eV) were also found between small polaron species and lithium vacancies, $[M_{M}^{\bullet}-V_{Li}^{\prime}]$, which suggests the trapping or coupling of these charge carriers in $Li_{1-x}MPO_4$.

(4) The calculated migration energies (0.7∼1.3 eV) for divalent antisite cations ($M_{Li}^{\bullet}$) jumping between two lithium sites down [010] channels suggests that such antisite defects would impede Li diffusion to varying degrees. However, the lowest antisite migration energy (0.7 eV) is for $LiFePO_4$, suggesting that any antisite defects in this system would have the least effect on lithium diffusion kinetics.

(5) Of the four systems, the weakest binding energies for all defect pair clusters were found for $LiFePO_4$. The overall trends in the energies of ion migration and defect association suggest higher lithium insertion/extraction rates, and thus better electrochemical performance, in $LiFePO_4$ compared with the other three systems.

(6) A variety of dopants with charges of +1 to +5 were examined for both Li^+ and M^{2+} substitution. Low favorable energies were found only for Na^+ substitution on the Li^+ site and isovalent dopants (e.g., Mg^{2+}) on the M^{2+} site. In contrast, supervalent doping (especially Ti^{4+} and Nb^{5+}) appears unfavorable on both Li^+ and M^{2+} sites in all four phases; the charge-compensation mechanism found for such doping in $LiMPO_4$ does not alter the M^{2+} valence state and hence is unlikely to contribute to high electronic conductivity. These results are in accord with recent experimental reports of unsuccessful incorporation of significant levels (>3%) of aliovalent dopants to enhance electronic conductivity.

Acknowledgment. We thank the EPSRC for funding as part of the Supergen Energy Storage Consortium (Grant EP/D031672/1). We are also grateful to J. Maier, C. Masquelier, and L. F. Nazar for useful discussions.

Supporting Information Available: List of potential parameters for hole species and dopant cations and comparison of calculated and experimental bond lengths for the four olivine phosphates $LiMPO_4$ (M = Mn, Fe, Co, and Ni). This information is available free of charge via the Internet at http: //pubs.acs.org.

CM801262X